Direct In Situ Mass Specific Absorption Spectra of Biomass Burning Particles Generated from Smoldering Hard and Softwoods

James G. Radney,[†][ID] Rian You,[†,‡] Michael R. Zachariah,[†,‡][ID] and Christopher D. Zangmeister[*,†][ID]

†Material Measurement Laboratory, National Institute of Standards and Technology, Gaithersburg, Maryland 20899, United States
‡Department of Chemistry and Biochemistry, University of Maryland, College Park, Maryland 20742, United States

S *Supporting Information*

ABSTRACT: Particles from smoldering biomass burning (BB) represent a major source of carbonaceous aerosol in the terrestrial atmosphere. In this study, mass specific absorption spectra of laboratory-generated smoldering wood particles (SWP) from 3 hardwood and 3 softwood species were measured in situ. Absorption data spanning from $\lambda = 500$ to 840 nm were collected using a photoacoustic spectrometer coupled to a supercontinuum laser with a tunable wavelength and bandwidth filter. SWP were size- (electrical mobility) and mass-selected prior to optical characterization allowing data to be reported as mass-specific absorption cross sections (MAC).

The median measured MAC at $\lambda = 660$ nm for smoldering oak particles was 1.1 (0.57/1.8) $\times 10^{-2}$ m^2 g^{-1} spanning from 83 femtograms (fg) to 517 fg (500 nm ≤ mobility diameter ≤950 nm), MAC values in parentheses are the 16th and 84th percentiles of the measured data (i.e., 1σ). The collection of all six wood species (Oak, Hickory, Mesquite, Western redcedar, Baldcypress, and Blue spruce) had median MAC values ranging from 1.4×10^{-2} m^2 g^{-1} to 7.9×10^{-2} m^2 g^{-1} at $\lambda = 550$ nm with absorption Ångström exponents (AAE) between 3.5 and 6.2. Oak, Western redcedar, and Blue spruce possessed statistically similar ($p > 0.05$) spectra while the spectra of Hickory, Mesquite, and Baldcypress were distinct ($p < 0.01$) as calculated from a point-by-point analysis using the Wilcox rank-sum test.
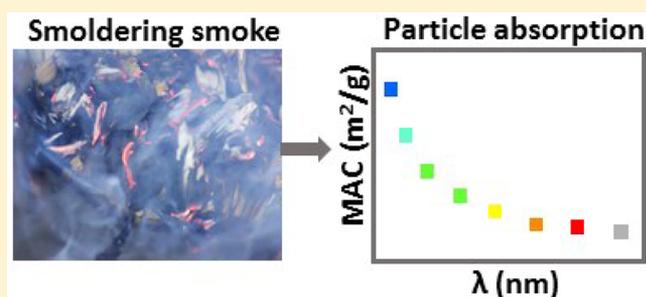
INTRODUCTION

Biomass burning (BB) is estimated to contribute >35% to the global emission of carbonaceous aerosol by mass.[1] The major particle-phase constituents generated from BB combustion can be optically categorized into 3 broad groups: black carbon (BC), absorbing organic carbon (brown carbon, BrC), and nonabsorbing organic carbon (OC).[2] The mix of BC, BrC, and OC emitted depends upon conditions with BC preferentially formed during flaming and BrC and OC during smoldering combustion.[3,4]

The net positive radiative forcing[5,6] of BC is second only to CO$_2$, due to its strong, and nearly wavelength independent, absorption and low single scattering albedo across the visible spectrum ($\lambda = 400$ to 700 nm).[7] BrC absorption is much lower than BC and is strongly wavelength dependent, being weak or negligible in the near-IR and significantly increasing toward the UV.[8] The BrC wavelength dependence introduces large uncertainties into radiative forcing calculations[4] with predictions of BrC's climate impact ranging from net neutral[9] to net positive.[10,11] One input into climate models are the BC and BrC mass-specific absorption cross sections (MAC, m^2 g^{-1}). Depending on the instrumentation and method used, MAC can take a variety of forms,

$$\text{MAC} = \frac{\alpha_{abs}}{N m_p} = \frac{C_{abs}}{m_p} = \frac{\alpha_{abs}}{\rho V} = \frac{\alpha_{abs}}{M} \qquad (1)$$

where α_{abs} (m^{-1}), N (m^{-3}), m_p (g), C_{abs} (m^2), ρ (kg m^{-3}), V (m^3 of aerosol per m^3 of air), and M (g of aerosol per m^3 of air) are the aerosol absorption coefficient, the aerosol number density, the average particle mass, the absorption cross section ($C_{abs} = \alpha_{abs}/N$), the average particle mass density, the volume fraction of aerosol particles and the mass concentration of aerosol particles ($M = N m_p = \rho V$), respectively. The corresponding units for each parameter are shown in parentheses. The wavelength dependent absorption is commonly described by the absorption Ångström exponent (AAE):

$$\text{MAC}_\lambda = \text{MAC}_{\lambda_0} \left(\frac{\lambda}{\lambda_0} \right)^{-\text{AAE}} \qquad (2)$$

where λ and λ_0 are an arbitrary wavelength in the spectrum and a reference wavelength, respectively. In this study, eq 2 has been defined by MAC, although C_{abs} or α_{abs} could also be used. Ångström exponents were originally used to describe the wavelength dependence of extinction for high albedo materials,[12] but have also been used to describe the wavelength dependence of particle absorption even though a single AAE

value may not accurately describe the entire spectrum; see Moosmüller, et. al (2011)[13] and references therein.

BB aerosol optical properties can be measured in the field during uncontrolled[14−16] or prescribed fires.[17,18] Laboratory measurements use more controlled combustion[4,19−25] or pyrolysis[26] conditions with known fuel types and quantities. BB MAC have been indirectly measured using two primary instrumental platforms: filters and photoacoustic spectroscopy (PAS). Filter measurements collect particles and low-volatility OC components and absorption is inferred either through changes in filter attenuation[24,27] (a surrogate for absorption) or extraction by solvents followed by subsequent measurement of the solution absorption spectrum with relatively high spectral resolution (<20 nm).[16,26,28] Filter-based measurements cannot completely capture aerosol MAC, as the method is not quantitative on a per mass basis due to challenges in measuring deposited particle mass, filter artifacts (multiple scattering, shadowing, evaporative loss, adsorptive gain, etc.), solvent extraction efficiencies, and the assumption that the absorption spectrum of the collected material is unaffected by solvation.

The second platform uses PAS to measure absorption coefficients and the average MAC for an entire population is determined indirectly using the third or fourth forms of eq 1 $\left(\text{MAC} = \frac{\alpha_{\text{abs}}}{\rho V} = \frac{\alpha_{\text{abs}}}{M} \right)$. Average density is either assumed or calculated from measured chemical composition mass fractions.[22,23] Volume distributions are inferred from the measured size distributions (assuming spherical particles). Mass concentrations are determined gravimetrically,[14,19−21,25] using an aerosol mass spectrometer[29] or a laser-induced incandescence instrument (elemental carbon only).[18] Each of the measured quantities requires separate instrumentation operated simultaneously and in parallel. This method is highly sensitive to the accuracy of ρ, V and M and any error in data collection or fitting amplifies MAC uncertainty without consideration to inherent particle variability.[19,22,23] Further, MAC values are typically reported at a single wavelength. When multiple wavelengths are available, AAEs are calculated from pairwise fits of the PAS data or from multiwavelength filter attenuation data in conjunction with PAS data to correct for filter biases.[30] Method uncertainties have led to conflicting interpretations on the influence of combustion conditions and/or fuel type on BB particle absorption.[22,31]

To ascertain the influence of wood specie on the optical properties of smoldering combustion, three conditions are required: (1) optimally controlled conditions to minimize intra- and interexperiment variability, (2) low measurement uncertainties relative to the intraexperiment and wood specie variation, and (3) quantification of experimental uncertainties (Type A and Type B) to isolate interspecie variation from method uncertainties. The current investigation measures the MAC of smoldering wood particles (SWP) that contain BrC under well-controlled conditions across a broad wavelength range for 6 fuel types using photoacoustic spectroscopy; however, unlike previous investigations, MAC was determined using the first form of eq 1 $\left(\text{MAC} = \frac{\alpha_{\text{abs}}}{Nm_{\text{p}}} \right)$; notably, α_{abs}, N, and m_{p} are all directly measured quantities.[32] Absorption data were collected for mobility- and mass-selected particles at 8 wavelengths between $\lambda = 500$ and 840 nm using a photoacoustic spectrometer (PA) and step-scanning a super-continuum laser coupled to a tunable wavelength and bandwidth filter. Wood specie variation was larger than

quantified method uncertainty and interexperiment variability facilitating determination of wood specie influence on MAC spectra on a statistical basis.

■ MATERIALS AND METHODS

A schematic of the experimental setup is shown in Figure 1 which includes components to generate and condition, size-
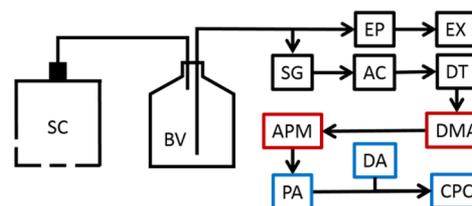

Figure 1. Experiment schematic. Black: aerosol generation and conditioning. Red: size and mass selection. Blue: spectroscopic characterization. Abbreviations: smoldering chamber (SC), 20 L buffer volume (BV), ejector pump (EP), exhaust (EX), silica gel diffusion dryer (SG), activated carbon diffusion dryer (AC), drying tube (DT), differential mobility analyzer (DMA), aerosol particle mass analyzer (APM), photoacoustic spectrometer (PA), dilution air (DA), and condensation particle counter (CPC).

and mass-select (differential mobility analyzer, DMA, and aerosol particle mass analyzer, APM, respectively) and measure the absorption spectra (photoacoustic spectrometer, PA) and number density (condensation particle counter, CPC) of the SWP; these components are shown with black, red, and blue outlines, respectively.

SWP Generation. Six wood species were investigated including hardwoods consisting of Oak (mixture of *Quercus falcata* and *Quercus alba*), Hickory (mixture of *Carya ovata* and *Carya texana*), and Mesquite (*Prosopis juliflora*) and softwoods of Western redcedar (*Thuja plicata*), Baldcypress (*Taxodium distichum*), and Blue spruce (*Picea pungens*). The Hickory, Mesquite, Western redcedar, and Baldcypress were sourced from commercially available wood chips. Oak chips and Blue spruce twigs were collected from the grounds of the National Institute of Standards and Technology (NIST) located in Gaithersburg, Maryland U.S.A. All samples were pretreated at 100 °C overnight to remove bulk water.[33]

Smoldering was initiated using in an in-house built combustor contained within a laboratory fume hood. The combustor consisted of a 0.95 L (1 qt) stainless steel can 10.8 cm tall and 12.38 cm in diameter with seven 0.556 cm diameter air holes (three on side wall and four at bottom center) to supply air. An exit port in the lid was fashioned from a 1.27 cm ($^1/_2$ in) NPT galvanized steel flange connected to a 1.27 cm ($^1/_2$ in) NPT galvanized steel tube and 0.952 cm ($^3/_8$ in) stainless steel tube. Using a downstream ejector pump, a constant and controlled amount of air (∼10 L min^{-1}) was pulled into the smoldering chamber via the air holes, over the smoldering wood, through the exit port and delivered to a 20 L glass carboy buffer volume; nominal carboy residence time was 2 min. All transfer lines consisted of conductive silicone tubing or stainless steel to minimize particle loss and deposition. For each run, ∼100 g of fuel was used. The fuel was ignited at the bottom of the smoldering chamber using a propane torch. SWP were observed in the buffer volume nearly immediately upon application of the heat source to the wood sample. Following the airflow recommendations of Ohlemiller,[34] stable smoldering was able to be maintained for up to 60 min. On rare occasions, size-
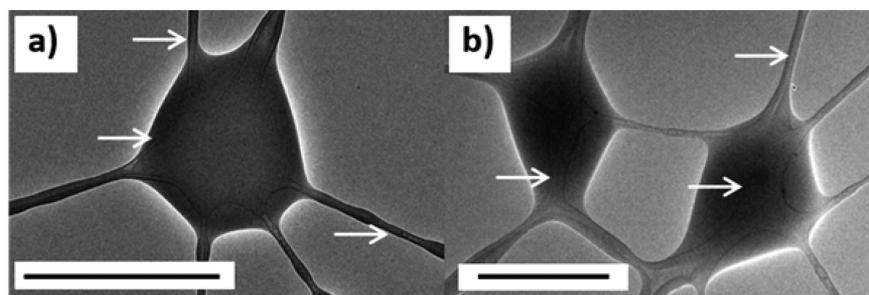
Figure 2. TEM images of collected from a) Oak and b) Blue spruce m_p = 270 fg (D_m = 750 nm) SWP. Liquid-like material forms coatings on the TEM grid and membranes at grid junctions. Scale bars are 1000 nm. White arrows point toward the underlying TEM grid.

flaming was visible in the combustor and limited to small parts of the sample, cessation was rapid due to limited O_2 (air flow was constant) resulting in continuation of smoldering.

SWP were sampled prior to the ejector pump at a flow rate of 0.5 L min^{-1}. Multiple steps were used to limit the impact of residual combustion gases and condensable water vapor and to maintain a constant relative humidity over the course of a single smoldering experiment. Residual combustion gases were removed by passing the particles through a diffusion dryer filled with activated carbon. Water vapor was removed by passing the particles through a diffusion dryer filled with silica gel desiccant and a monotube gas dryer. Silica desiccant was changed prior to each experiment. Under these conditions the relative humidity in the DMA was maintained at <8%.

Size and Mass Classification. SWP were size-selected at a given mobility diameter (D_m) using an electrostatic classifier with long DMA column that was operated with an aerosol flow of 0.5 L min^{-1} and a sheath flow of 2.5 L min^{-1}. Particles were mass selected using an APM that was operated either in scanning mode for the determination of the average mass of particles with $q \geq +1$—see Radney and Zangmeister (2016)[35]—or static mode to measure absorption spectra where the APM was set to the average mass of the $q = +1$ distribution.

This combination of DMA-APM also enables determination of the effective density (ρ_{eff})[36,37] from the following:

$$\rho_{eff} = \frac{6m_p}{\pi D_m^3}$$

(3)

where m_p is the average mass of $q = +1$ charged particles determined from the mass distribution measured by the APM.

Absorption Measurements. The absorption coefficients of size- and mass-selected SWP were measured at eight wavelengths spanning from λ = 500 to 840 nm using a PA with a supercontinuum laser and tunable wavelength and bandwidth filter. The reader is directed to Radney and Zangmeister (2015)[38] for a detailed description on the determination of α_{abs} using the supercontinuum PA. Similar to this previous investigation, wavelength regions were randomized at the beginning of each experiment to reduce systematic bias as a result of collection order.

AAEs were calculated by fitting median MAC values to eq 2 with λ_0 = 550 nm; reported uncertainties represent fits of the 16th and 84th percentile data (see Supporting Information, SI, for a full discussion of data analysis). To test for spectral similarity, the Wilcox rank-sum test was performed on a wavelength-by-wavelength basis using postprocessed data; uncertainties were asymmetric about the median and the number of data points in each spectrum were not equivalent

necessitating the use of a nonparametric test. Spectra with >4 out of 8 data points possessing a statistically significant ($p <$ 0.01) difference from all other spectra were considered distinct.

TEM Characterization. Size- and mass-selected SWP were collected on TEM grids (200-mesh copper grids coated with lacey carbon film) using an electrostatic aerosol precipitator at −9.3 kV collection voltage, and an aerosol flow of 0.5 L min^{-1}. TEM images were collected at an accelerating voltage of 200 kV.

RESULTS

Particle Characterization. Low temperature combustion produces primarily liquid particles formed from the condensation of gaseous organic compounds minimizing the formation of BC.[27] Figure 2 shows TEM images of Oak and Blue spruce SWP at m_p = 270 fg (D_m = 750 nm) and the white arrows designate selected regions of the underlying TEM grid. No aggregated solid particles (i.e., BC)[39,40] were observed. Instead, the grids are nearly universally coated by a thin liquid layer with membranes spanning the individual TEM grid fibers suggesting the particles conform to the grid upon impact, similar to previous observations of BB particles[41] (see SI for additional TEM images). For reference, the scale bars in Figure 2 correspond to 1000 nm and the selected particle mobility diameters were 750 nm. Thus, each image likely contains material from a single particle (Oak, Figure 3a) or a couple of particles (Blue spruce, Figure 3b).

SWP Density Measurements. Particle densities from SWP were determined for the six wood species under investigation using mass distributions from mobility selected particles.[32,36,37] Particle densities ranged between 1.31 g cm^{-3} for Blue spruce and Baldcypress up to 1.51 g cm^{-3} for Mesquite, see Table 1. These values are similar to densities derived from mobility and microbalance measurements of organic carbon from BB and densities calculated from compositional analysis of particles collected during flaming combustion from a variety of North American biomass.[14,22]

Smoldering Wood Absorption. Wood smoldering produced particles across a broad mass range. Particles were initially mobility classified (D_m) and subsequently mass selected (m_p) prior to entering the PAS, allowing all measurements to be reported on a per mass basis (an SI traceable quantity) versus electrical mobility which is morphology dependent. SWP were first measured at a single wavelength (660 nm) to study particle absorption as a function of m_p, see Figure 3. The MAC of oak SWP was 1.1 (0.57/1.8) × 10^{-2} m^2 g^{-1} at λ = 660 nm for particles between 83 fg and 517 fg (500 nm $\leq D_m \leq$ 950 nm). Each data point represents an independent experiment where the wood sample was replaced and smoldering was initiated.
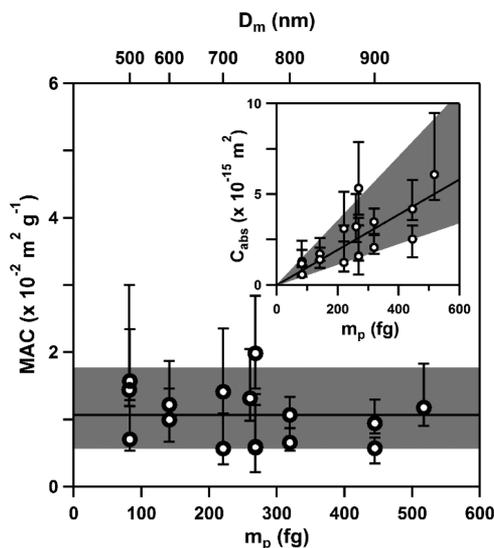
Figure 3. Median MAC of oak SWP as a function of particle mass (bottom axis) and mobility diameter (top axis). Uncertainties in MAC represent the 16th and 84th percentiles (i.e., 1σ). Solid black line and greyed area represent the median MAC and uncertainty across all measured data at all masses, respectively. Inset shows C_{abs} as a function of particle mass (m_p). Solid black line represents fit of data and greyed area represents uncertainty of fit. Slope is MAC for the range of measured m_p.

The variability in measured MAC is dominated by interexperiment variability (e.g., sample-to-sample variability) and not intraexperiment variability. The solid black line and shaded area represent the measured median (1.1×10^{-2} m^2 g^{-1}) and the 16th (0.57×10^{-2} m^2 g^{-1}) and 84th (1.8×10^{-2} m^2 g^{-1}) percentiles (i.e., 1σ), respectively, across all data. The inset of Figure 3 shows C_{abs} as a function of mass, the slope of the linear fit is MAC for the range of measured m_p $(9.7 \pm 1.0) \times 10^{-3}$ m^2 g^{-1}; uncertainty is 1 standard deviation of the linear fit of C_{abs} vs m_p without regard to underlying C_{abs} uncertainties. Importantly, within experimental uncertainties, SWP MAC is independent of m_p across the measured mass range (i.e., particles are behaving as volume absorbers).[42] Considering the absolute magnitude of MAC measured at λ = 660 nm, the linear relationship of C_{abs} with m_p will hold across the entire range of measured wavelengths (see the SI).

For Oak SWP, C_{abs} at λ = 660 nm scales linearly with mass thereby demonstrating that only a single size and mass combination was necessary to determine MAC for each wood specie. Spectroscopic measurements were performed where the largest mass concentration (D_m = 750 nm, $m_p \approx$ 270 fg) and hence absorption coefficients were obtained, as shown by eq 1:

$\alpha_{abs} = M \cdot$ MAC. The measured values of MAC were similar enabling the single size and mass combination to be used for all wood species.

Figure 4 shows the MAC spectra of mass-selected (D_m = 750 nm) SWP for six wood species; data points represent the median measured data collected from between 15 and 70 absorption spectra per smoldering experiment. Shaded regions represent the 16th and 84th percentiles (i.e., 1σ). Solid and dashed lines represent AAE fits to the median and 16th and 84th percentiles, respectively; median MAC at λ = 550 nm (MAC$_{\lambda,0}$ in eq 2) and AAE are shown in Table 1 with percentiles shown in parentheses. All data were well described using eq 2 with the exception of Baldcypress. Equation 2 is typically only used in discrete pairwise calculations due to a lack of spectral resolution. The presented in situ SWP absorption data have the highest reported spectral resolution to date and all of the measured data were used to fit to the noted power law dependence. However, the spectra may indicate the presence of more complex wavelength dependencies than can be described by a single power law, suggesting that multiple AAEs may be required.[13]

The measured SWP MAC were 2 orders of magnitude lower than the cited MAC of BC[7,45] with the highest measured median MAC = 7.9 (6.0/12) $\times 10^{-2}$ m^2 g^{-1} for Mesquite at λ = 550 nm; values in parentheses are the 16th and 84th percentiles of the measured data. The strongest absorbing particles, Mesquite and Hickory, have MAC values about 5 times greater than that of the weakest absorbers, Oak and Western redcedar. The MAC and AAE values of the 6 wood species measured compare well to the suggested values by Reid et al. (2005)[46] who conducted an extensive review of smoldering forest fire data and concluded that the MAC of particles emitted during smoldering are <0.3 m^2 g^{-1} at λ = 550 nm; these data suggest that a generalized wood-type independent value for smoldering MAC of <0.1 m^2 g^{-1} may be more accurate. Previously, Chakrabarty et al. (2016)[19] measured a MAC of 3 $\times$ 10^{-2} m^2 g^{-1} to 7 $\times$ 10^{-2} m^2 g^{-1} at λ = 532 nm for smoldering peat samples (50% moisture content) while Hoffer et al. (2006)[14] measured MAC of 2.9 $\times$ 10^{-2} m^2 g^{-1} to 3.1 $\times$ 10^{-2} m^2 g^{-1} at λ = 532 nm for fine-fraction isolates of Amazon basin biomass-burning aerosol. Both of these previous values compare well to the results reported in this study.

BC Contribution. Following the convention used in other investigations, it can be assumed that BrC contained within SWP does not absorb significantly in the in near-IR spectral region (λ = 840 nm) and that all absorption at 840 nm corresponds to BC. Using this assumption, the estimated BC contribution is a maximum of 0.4% by mass (Mesquite, see Table 1), but is likely closer to 0.1% by mass by taking into

Table 1. Measured Effective Density, Median MAC, AAE, and Calculated Mass % BC, BrC MAC, and AAE

species	effective density (g cm^{-3})	median MAC ($\times 10^{-2}$ m^2 g^{-1})^a	AAE^a	mass % BC^b	BrC MAC ($\times 10^{-2}$ m^2 g^{-1})^c	BrC AAE^c
Oak^d	1.41 (0.04)	2.5 (0.76/4.3)	5.5 (4.8/4.7)	0.09	1.1	11
Hickory^d	1.44 (0.05)	7.0 (4.0/11)	3.8 (4.0/4.7)	0.4	3.7	7.0
Mesquite^d	1.51 (0.03)	7.9 (6.0/12)	3.5 (3.5/4.2)	0.4	4.6	7.2
Western redcedar^e	1.36 (0.03)	1.4 (0.81/2.6)	5.2 (5.6/4.3)	0.07	0.77	10
Blue spruce^e	1.35 (0.02)	1.4 (0.039/4.7)	6.2 (3.9/3.4)	0.09	0.069	35
Baldcypress^e	1.35 (0.01)	4.3 (3.0/6.6)	4.1 (3.6/5.5)	0.3	0.90	16

$^a\lambda$ = 550 nm value calculated from AAE fit (eq 2) of average values spanning λ = 500 to 840 nm. Values in parentheses are the values from fits of the 16th and 84th percentile data. ^{b}Upper bound of BC % mass. Assumes no refractive index matching. $^c\lambda$ = 550 nm value calculated assuming all absorption at λ = 840 nm is due to BC. See discussion in text. ^{d}Hardwood. ^{e}Softwood.
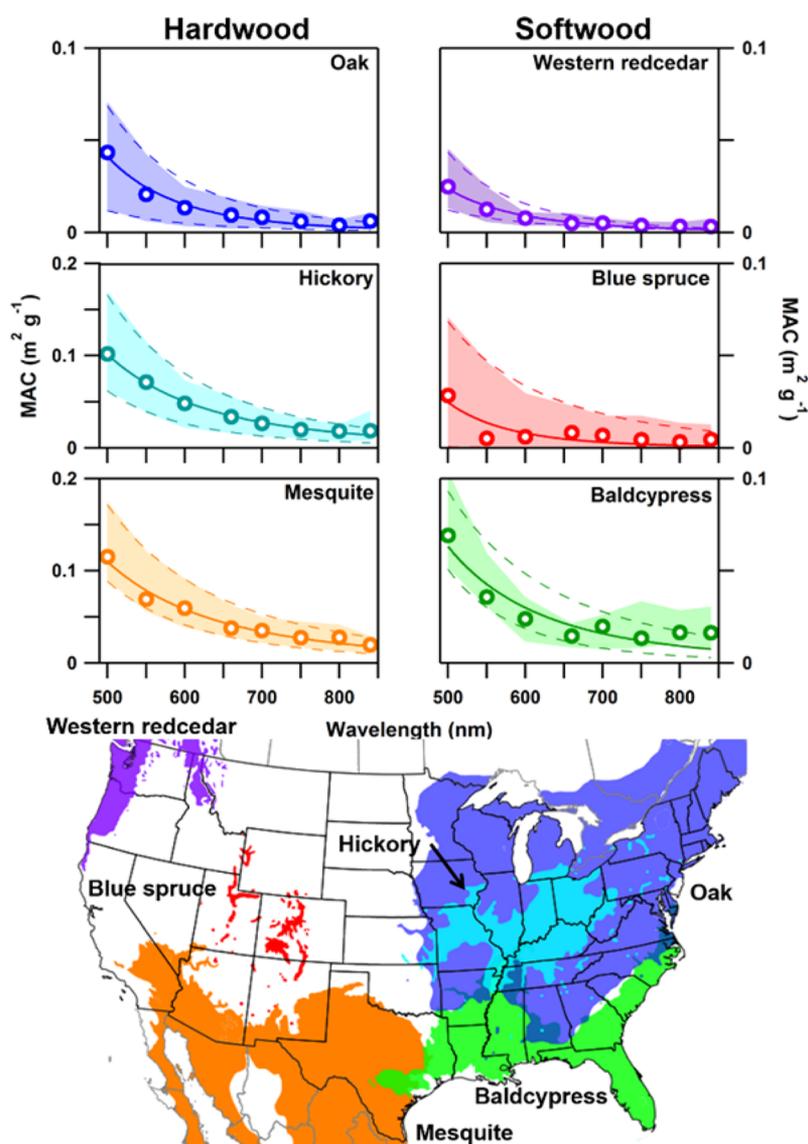
Figure 4. Measured MAC as a function of wavelength for SWP from six species of wood. Open circles and shaded areas represent the median MAC values and the 16th and 84th percentiles (i.e., 1σ) at each wavelength, respectively; solid and dashed lines represent AAE fits to the median and 16th and 84th percentile values, respectively. Wood species distribution is shown on map at bottom and correspond to the colors of each species absorption spectrum. Map was generated from level 1 global administrative area basemaps[43] overlaid with tree species range maps[44] using geographic information systems software.

account refractive index matching[47,48] (see SI). If present, the BC per particle is below the detection limit of even the most sensitive current in situ BC techniques, consistent with the lack of observed BC in the presented SWP TEM images. Subtracting the noted BC spectral contribution increased the calculated AAE to between 7.0 and 35 (see Table 1) similar to results from smoldering peat using the same fitting routine.[4]

■ DISCUSSION

The present data, to our knowledge, represent the first direct, in situ MAC spectra of SWP. MAC is directly calculated from three measured quantities (absorption coefficients, mass and number density) that, more importantly, do not require any assumptions of particle chemical composition, material density, or morphology as is required for filter-based solvent-extraction or compositional analysis measurements. In this investigation, the instrumental calibration uncertainties are on the order of few percent (see SI). As a result, unlike these other methods,

the MAC and wavelength dependencies are dominated by the variability in particle absorption (Type A uncertainty) allowing for quantitative comparison between spectra.

Using the Wilcox rank-sum test, point-by-point comparison of the individual SWP absorption spectra reveals that Oak, Western redcedar, and Blue spruce are statistically similar ($p > 0.05$) while Hickory, Mesquite, and Baldcypress were each distinct ($p < 0.01$); see SI for analysis statistics. The data suggest that, for smoldering biomass, MAC, and spectral shape can be species dependent.

The measured absorption spectra are likely influenced by wood composition. Wood is composed of lignin, cellulose, hemicellulose (HC), and extractives. Lignin is a phenolic biopolymer residing between wood cell walls that thermally degrades slowly between 225 and 700 °C.[33,49] Cellulose forms the fibrous tissue in wood and is composed of up to 10^3 glucose units arranged in a multilayered, hydrogen bonded structure that make it thermally stable up to 800 °C.[33] HC comprises

wood cell walls that accounts for up to 50% of wood's mass. Nearly 90% of the HC in deciduous trees (encompassing most hardwood species) are xylans, a family of xylose polysaccharides, that thermally degrade between 200 and 300 °C.[33] Softwood species HC is additionally composed of glucomannan (a branched polysaccharide) and arabinogalactan (an arabinose and galactose monosaccharide), both of which thermally degrade over the same temperature range as xylans. Extractives are nonstructural constituents that are chemically distinct for each wood specie that account for ∼1% by mass. Unlike structural components, the composition and mass percentage of extractives may vary greatly in different parts of biomass (wood, bark, needles, leaves). Hardwood extractives consist of fatty acids and phenolic compounds (stilbenes, lignans, etc.) while softwood extractives are mostly resins of terpenes and terpene derivatives.[33]

Thermocouple readings taken within the smoldering chamber were <280 °C, below the flaming initiation temperature for hardwoods (300 °C) and softwoods (350 °C), minimizing BC formation.[50] Thermal decomposition via smoldering is initiated by xylose thermolysis, forming and releasing acetic and formic acids. Both acids catalyze HC thermal decomposition releasing a mixture of gaseous products and condensable species.[51] The products formed from HC and extractive thermal degradation and release have been shown to be chemically distinct for each wood specie. For example, the condensed phase emissions of Scots pine (*Pinus sylvestris*) heated between 200 and 260 °C measured 21% H_2O, 8% acetic acid, 5% formic acid, nearly 4% methanol and the balance was a mixture of organic species.[52] Smoldering Northern spruce (*Picea abies*) thermal decomposition products were 90% acetic and formic acids by mass with a few percent each of fatty acids, resins, and phenolic compounds.[53] Lastly, studies that heated a range of biomass types between 250 and 300 °C collected light brown, viscous tar-like products, consistent with the presented TEM images and spectroscopic measurements.[52]

Previous studies of BB have been divided whether fuel type or combustion conditions have the largest influence on particle optical properties. Correlations of the light absorbing carbon contained in aerosol and the calculated imaginary refractive index have been demonstrated,[22] while other studies suggest that particle absorption is independent of biomass fuel type but dependent on burn conditions (ratio of smoldering to flaming combustion).[31] The data reported in this investigation of particles produced from controlled low temperature smoldering indicates that both MAC and AAE can be influenced by fuel type. Measured particle absorption spectra from six wood species showed that the SWP MAC and spectral shape of three species were statistically distinct while three were statistically similar. The six wood species had measured median MAC values spanning between 0.014 m^2 g^{-1} and 0.079 m^2 g^{-1} at λ = 550 nm and AAEs ranging from 3.5 (Mesquite) to 6.2 (Blue spruce).

■ ASSOCIATED CONTENT

Ⓢ Supporting Information

The Supporting Information is available free of charge on the ACS Publications website at DOI: 10.1021/acs.est.7b00810.

> Additional TEM images of Oak and Blue spruce particles. Description of the data analysis procedure and Oak SWP smoldering stability. Calculations of Oak refractive index at λ = 660 nm from C_{abs} data. The refractive index is then extended to λ = 500 and 840 nm to demonstrate MAC mass independence over the range of particle sizes measured. Details on the calculation of BC mass fraction and instrumental uncertainties. Spectral correlation tables for the Wilcox Rank-sum calculations (PDF)

■ AUTHOR INFORMATION

Corresponding Author
*Phone: (301)975-8709; fax: (301)975-3670; e-mail: cdzang@nist.gov (C.D.Z.).

ORCID Ⓘ
James G. Radney: 0000-0001-7324-8769
Michael R. Zachariah: 0000-0002-4115-3324
Christopher D. Zangmeister: 0000-0002-6026-9293

Author Contributions
The manuscript was written through contributions of all authors. All authors have given approval of the final version of the manuscript.

Notes

■ REFERENCES

(1) IPCC, Changes in Atmospheric Constituents and in Radiative Forcing. In *Contribution of Working Group I to the Fourth Assessment Report of the Intergovernmental Panel on Climate Change, 2007*; Solomon, S., Qin, D., Manning, M., Chen, Z., Marquis, M., Averyt, K. B., Tignor, M., Miller, H. L., Eds.; Cambridge University Press: Cambridge/New York, 2007; pp 129−234.

(2) Pöschl, U. Atmospheric aerosols: Composition, transformation, climate and health effects. *Angew. Chem., Int. Ed.* **2005**, *44* (46), 7520−7540.

(3) Martinsson, J.; Eriksson, A. C.; Nielsen, I. E.; Malmborg, V. B.; Ahlberg, E.; Andersen, C.; Lindgren, R.; Nyström, R.; Nordin, E. Z.; Brune, W. H.; Svenningsson, B.; Swietlicki, E.; Boman, C.; Pagels, J. H. Impacts of combustion conditions and photochemical processing on the light absorption of biomass combustion aerosol. *Environ. Sci. Technol.* **2015**, *49* (24), 14663−14671.

(4) Chakrabarty, R. K.; Moosmuller, H.; Chen, L. W. A.; Lewis, K.; Arnott, W. P.; Mazzoleni, C.; Dubey, M. K.; Wold, C. E.; Hao, W. M.; Kreidenweis, S. M. Brown carbon in tar balls from smoldering biomass combustion. *Atmos. Chem. Phys.* **2010**, *10* (13), 6363−6370.

(5) Sato, M.; Hansen, J.; Koch, D.; Lacis, A.; Ruedy, R.; Dubovik, O.; Holben, B.; Chin, M.; Novakov, T. Global atmospheric black carbon inferred from AERONET. *Proc. Natl. Acad. Sci. U. S. A.* **2003**, *100* (11), 6319−6324.

(6) Bond, T. C.; Doherty, S. J.; Fahey, D. W.; Forster, P. M.; Berntsen, T.; DeAngelo, B. J.; Flanner, M. G.; Ghan, S.; Kärcher, B.; Koch, D.; Kinne, S.; Kondo, Y.; Quinn, P. K.; Sarofim, M. C.; Schultz, M. G.; Schulz, M.; Venkataraman, C.; Zhang, H.; Zhang, S.; Bellouin, N.; Guttikunda, S. K.; Hopke, P. K.; Jacobson, M. Z.; Kaiser, J. W.; Klimont, Z.; Lohmann, U.; Schwarz, J. P.; Shindell, D.; Storelvmo, T.; Warren, S. G.; Zender, C. S. Bounding the role of black carbon in the climate system: A scientific assessment. *J. Geophys. Res.: Atmos.* **2013**, *118*, 5380−5552.

(7) Bond, T. C.; Bergstrom, R. W. Light absorption by carbonaceous particles: An investigative review. *Aerosol Sci. Technol.* **2006**, *40* (1), 27−67.

(8) Andreae, M. O.; Gelencser, A. Black carbon or brown carbon? The nature of light-absorbing carbonaceous aerosols. *Atmos. Chem. Phys.* **2006**, *6* (10), 3131−3148.

(9) IPCC, *Climate Change 2013: The Physical Science Basis. Contribution of Working Group I to the Fifth Assessment Report of the Intergovernmental Panel on Climate Change*; Cambridge University Press: Cambridge/New York, 2013; p 1535.

(10) Jacobson, M. Z. Effects of biomass burning on climate, accounting for heat and moisture fluxes, black and brown carbon, and cloud absorption effects. *J. Geophys. Res.: Atmos.* **2014**, *119* (14), 8980−9002.

(11) Feng, Y.; Ramanathan, V.; Kotamarthi, V. R. Brown carbon: a significant atmospheric absorber of solar radiation? *Atmos. Chem. Phys.* **2013**, *13* (17), 8607−8621.

(12) Ångström, A. On the atmospheric transmission of sun radiation and on dust in the air. *Geogr. Ann.* **1929**, *11*, 156−166.

(13) Moosmüller, H.; Chakrabarty, R. K.; Ehlers, K. M.; Arnott, W. P. Absorption Ångström coefficient, brown carbon, and aerosols: basic concepts, bulk matter, and spherical particles. *Atmos. Chem. Phys.* **2011**, *11* (3), 1217−1225.

(14) Hoffer, A.; Gelencsér, A.; Guyon, P.; Kiss, G.; Schmid, O.; Frank, G. P.; Artaxo, P.; Andreae, M. O. Optical properties of humic-like substances (HULIS) in biomass-burning aerosols. *Atmos. Chem. Phys.* **2006**, *6* (11), 3563−3570.

(15) O'Neill, N. T.; Eck, T. F.; Holben, B. N.; Smirnov, A.; Royer, A.; Li, Z. Optical properties of boreal forest fire smoke derived from Sun photometry. *J. Geophys. Res.: Atmos.* **2002**, *107* (D11), 6-1−6-19.

(16) Srinivas, B.; Rastogi, N.; Sarin, M. M.; Singh, A.; Singh, D. Mass absorption efficiency of light absorbing organic aerosols from source region of paddy-residue burning emissions in the Indo-Gangetic Plain. *Atmos. Environ.* **2016**, *125*, 360−370.

(17) Lee, S.; Baumann, K.; Schauer, J. J.; Sheesley, R. J.; Naeher, L. P.; Meinardi, S.; Blake, D. R.; Edgerton, E. S.; Russell, A. G.; Clements, M. Gaseous and particulate emissions from prescribed burning in Georgia. *Environ. Sci. Technol.* **2005**, *39* (23), 9049−9056.

(18) Holder, A. L.; Hagler, G. S. W.; Aurell, J.; Hays, M. D.; Gullett, B. K. Particulate matter and black carbon optical properties and emission factors from prescribed fires in the southeastern United States. *J. Geophys. Res.: Atmos.* **2016**, *121* (7), 3465−3483.

(19) Chakrabarty, R. K.; Gyawali, M.; Yatavelli, R. L. N.; Pandey, A.; Watts, A. C.; Knue, J.; Chen, L. W. A.; Pattison, R. R.; Tsibart, A.; Samburova, V.; Moosmüller, H. Brown carbon aerosols from burning of boreal peatlands: microphysical properties, emission factors, and implications for direct radiative forcing. *Atmos. Chem. Phys.* **2016**, *16* (5), 3033−3040.

(20) Chen, L. W. A.; Moosmüller, H.; Arnott, W. P.; Chow, J. C.; Watson, J. G.; Susott, R. A.; Babbitt, R. E.; Wold, C. E.; Lincoln, E. N.; Hao, W. M. Particle emissions from laboratory combustion of wildland fuels: In situ optical and mass measurements. *Geophys. Res. Lett.* **2006**, *33* (4), L04803.

(21) Chen, L. W. A.; Moosmüller, H.; Arnott, W. P.; Chow, J. C.; Watson, J. G.; Susott, R. A.; Babbitt, R. E.; Wold, C. E.; Lincoln, E. N.; Hao, W. M. Emissions from laboratory combustion of wildland fuels: Emission factors and source profiles. *Environ. Sci. Technol.* **2007**, *41* (12), 4317−4325.

(22) Levin, E. J. T.; McMeeking, G. R.; Carrico, C. M.; Mack, L. E.; Kreidenweis, S. M.; Wold, C. E.; Moosmüller, H.; Arnott, W. P.; Hao, W. M.; Collett, J. L., Jr.; Malm, W. C. Biomass burning smoke aerosol properties measured during Fire Laboratory at Missoula Experiments (FLAME). *J. Geophys. Res.* **2010**, *115* (D18), D18210.

(23) Mack, L. A.; Levin, E. J. T.; Kreidenweis, S. M.; Obrist, D.; Moosmüller, H.; Lewis, K. A.; Arnott, W. P.; McMeeking, G. R.; Sullivan, A. P.; Wold, C. E.; Hao, W. M.; Collett, J. L., Jr; Malm, W. C. Optical closure experiments for biomass smoke aerosols. *Atmos. Chem. Phys.* **2010**, *10* (18), 9017−9026.

(24) Pandey, A.; Pervez, S.; Chakrabarty, R. K. Filter-based measurements of UV−vis mass absorption cross sections of organic carbon aerosol from residential biomass combustion: Preliminary findings and sources of uncertainty. *J. Quant. Spectrosc. Radiat. Transfer* **2016**, *182*, 296−304.

(25) Hungershoefer, K.; Zeromskiene, K.; Iinuma, Y.; Helas, G.; Trentmann, J.; Trautmann, T.; Parmar, R. S.; Wiedensohler, A.; Andreae, M. O.; Schmid, O. Modelling the optical properties of fresh biomass burning aerosol produced in a smoke chamber: results from the EFEU campaign. *Atmos. Chem. Phys.* **2008**, *8* (13), 3427−3439.

(26) Chen, Y.; Bond, T. C. Light absorption by organic carbon from wood combustion. *Atmos. Chem. Phys.* **2010**, *10* (4), 1773−1787.

(27) Saleh, R.; Hennigan, C. J.; McMeeking, G. R.; Chuang, W. K.; Robinson, E. S.; Coe, H.; Donahue, N. M.; Robinson, A. L. Absorptivity of brown carbon in fresh and photo-chemically aged biomass-burning emissions. *Atmos. Chem. Phys.* **2013**, *13* (15), 7683−7693.

(28) Kirchstetter, T. W.; Novakov, T.; Hobbs, P. V. Evidence that the spectral dependence of light absorption by aerosols is affected by organic carbon. *J. Geophys. Res.: Atmos.* **2004**, *109*, D21.

(29) Barnard, J. C.; Volkamer, R.; Kassianov, E. I. Estimation of the mass absorption cross section of the organic carbon component of aerosols in the Mexico City Metropolitan Area. *Atmos. Chem. Phys.* **2008**, *8* (22), 6665−6679.

(30) Ajtai, T.; Filep, Á.; Utry, N.; Schnaiter, M.; Linke, C.; Bozóki, Z.; Szabó, G.; Leisner, T. Inter-comparison of optical absorption coefficients of atmospheric aerosols determined by a multi-wavelength photoacoustic spectrometer and an Aethalometer under sub-urban wintry conditions. *J. Aerosol Sci.* **2011**, *42* (12), 859−866.

(31) Saleh, R.; Robinson, E. S.; Tkacik, D. S.; Ahern, A. T.; Liu, S.; Aiken, A. C.; Sullivan, R. C.; Presto, A. A.; Dubey, M. K.; Yokelson, R. J.; Donahue, N. M.; Robinson, A. L. Brownness of organics in aerosols from biomass burning linked to their black carbon content. *Nat. Geosci.* **2014**, *7* (9), 647−650.

(32) Radney, J. G.; Ma, X.; Gillis, K. A.; Zachariah, M. R.; Hodges, J. T.; Zangmeister, C. D. Direct measurements of mass-specific optical cross sections of single component aerosol mixtures. *Anal. Chem.* **2013**, *85* (17), 8319−8325.

(33) Tumuluru, J. S.; Sokhansanj, S.; Hess, J. R.; Wright, C. T.; Boardman, R. D. A review on biomass torrefaction process and product properties for energy applications. *Ind. Biotechnol.* **2011**, *7* (5), 384−401.

(34) Ohlemiller, T. J. Smoldering Combustion Propagation On Solid Wood. *Fire Saf. Sci.* **1991**, *3*, 565−574.

(35) Radney, J. G.; Zangmeister, C. D. Practical limitations of aerosol separation by a tandem differential mobility analyzer−aerosol particle mass analyzer. *Aerosol Sci. Technol.* **2016**, *50* (2), 160−172.

(36) Park, K.; Cao, F.; Kittelson, D. B.; McMurry, P. H. Relationship between particle mass and mobility for diesel exhaust particles. *Environ. Sci. Technol.* **2003**, *37* (3), 577−583.

(37) McMurry, P. H.; Wang, X.; Park, K.; Ehara, K. The relationship between mass and mobility for atmospheric particles: A new technique for measuring particle density. *Aerosol Sci. Technol.* **2002**, *36* (2), 227−238.

(38) Radney, J. G.; Zangmeister, C. D. Measurement of gas and aerosol phase absorption spectra across the Visible and near-IR using Supercontinuum photoacoustic spectroscopy. *Anal. Chem.* **2015**, *87*, 7356−7363.

(39) Reid, J. S.; Koppmann, R.; Eck, T. F.; Eleuterio, D. P. A review of biomass burning emissions part II: intensive physical properties of biomass burning particles. *Atmos. Chem. Phys.* **2005**, *5* (3), 799−825.

(40) Buseck, P. R.; Adachi, K.; Gelencsér, A.; Tompa, E.; Pósfai, M. Ns-Soot: A material-based term for strongly light-absorbing carbonaceous particles. *Aerosol Sci. Technol.* **2014**, *48* (7), 777−788.

(41) Subramanian, R.; Roden, C. A.; Boparai, P.; Bond, T. C. Yellow beads and missing particles: Trouble ahead for filter-based absorption measurements. *Aerosol Sci. Technol.* **2007**, *41* (6), 630−637.

(42) Sun, H.; Biedermann, L.; Bond, T. C. Color of brown carbon: A model for ultraviolet and visible light absorption by organic carbon aerosol. *Geophys. Res. Lett.* **2007**, *34*, L17813.

(43) Hijmans, R. GADM Database of Global Administrative Areas. http://gadm.org (July 27, 2016).

(44) U. S. Geological Survey, Digital representation of "Atlas of United States Trees" by Little, E. L., Jr. http://gec.cr.usgs.gov/data/little (July 27, 2016).

(45) You, R.; Radney, J. G.; Zachariah, M. R.; Zangmeister, C. D. Measured wavelength-dependent absorption enhancement of internally mixed black carbon with absorbing and nonabsorbing materials. *Environ. Sci. Technol.* **2016**, *50* (15), 7982−7990.

(46) Reid, J. S.; Eck, T. F.; Christopher, S. A.; Koppmann, R.; Dubovik, O.; Eleuterio, D. P.; Holben, B. N.; Reid, E. A.; Zhang, J. A review of biomass burning emissions part III: intensive optical properties of biomass burning particles. *Atmos. Chem. Phys.* **2005**, *5* (3), 827−849.

(47) Jacobson, M. Z. A physically-based treatment of elemental carbon optics: Implications for global direct forcing of aerosols. *Geophys. Res. Lett.* **2000**, *27* (2), 217−220.

(48) Yablonovitch, E. Statistical ray optics. *J. Opt. Soc. Am.* **1982**, *72* (7), 899−907.

(49) Yang, H.; Yan, R.; Chen, H.; Lee, D. H.; Zheng, C. Characteristics of hemicellulose, cellulose and lignin pyrolysis. *Fuel* **2007**, *86* (12−13), 1781−1788.

(50) Babrauskas, V. *Ignition of Wood: A Review of the State of the Art*; Interflam 2001, London, 2001; Interscience Communications Limited: London, 2001; pp 71−88.

(51) Bourgois, J.; Guyonnet, R. Characterization and analysis of torrefied wood. *Wood Sci. Technol.* **1988**, *22* (2), 143−155.

(52) Esteves, B. M.; Pereira, H. M. Wood modification by heat treatment: A review. *BioResources* **2009**, *4* (1), 370−404.

(53) Alen, R.; Kotilainen, R.; Zaman, A. Thermochemical behavior of Norway spruce (Picea abies) at 180−225 degrees C. *Wood Sci. Technol.* **2002**, *36* (2), 163−171.